Development of Single-Crystal Ni-Base Superalloys Based on Multi-criteria Numerical Optimization and Efficient Use of Refractory Elements

M. MARKL, A. MÜLLER, N. RITTER, M. HOFMEISTER, D. NAUJOKS, H. SCHAAR, K. ABRAHAMS, J. FRENZEL, A.P.A. SUBRAMANYAM, A. LUDWIG, J. PFETZING-MICKLICH, T. HAMMERSCHMIDT, R. DRAUTZ, I. STEINBACH, R. RETTIG, R.F. SINGER, and C. KÖRNER

The development of new Ni-base superalloys with a complex composition consisting of eight or more alloying elements is a challenging task. The experimental state-of-the-art development cycle is based on the adaption of already existing compositions. Although new alloy compositions with potentially improved material properties are expected to be similar to already known superalloys, this procedure impedes efficiently finding these compositions in the large multi-dimensional design-space of all alloying elements. Modern alloy development combines numerical optimization methods with experimental validation to guide the development towards promising compositions. In this work, an improved numerical multi-criteria optimization tool using CALPHAD calculations and semi-empirical models for alloy development is presented. The model improvements to its predecessor are described and the successful application for the development of rhenium-free single-crystal Ni-base superalloys ERBO/13 and ERBO/15 is revisited. The optimization tool is described and the designed alloys are discussed regarding phase stability. Finally, a possible phase stability model extending the optimization tool and improving the alloy composition predictions is presented.

I. INTRODUCTION

DESIGNING new single-crystal Ni-base superalloy is a challenge due to competitive requirements on the material properties and the complexity of the material composition with eight or more alloying elements. Additionally, modifying a single element concentration usually influences more than one alloy property and the identification of individual effects is difficult. State-of-the-art alloy development comprises targeted adaption of existing alloy compositions for experimental testing. Consequently, alloy compositions of potentially improved material properties within the huge design-space spanned by all alloying elements are widely unexplored until today.

Modern alloy development combines numerical optimization methods with experimental validation to guide the development towards promising compositions. Instead of a single alloy composition which satisfies all multiple optimization criteria in a multi-component design-space, there exist a number of alloy compositions representing the Pareto front. All compositions on the Pareto front are optimal in the sense that it is not possible to improve one criterion without worsening another. Numerical approaches now try to determine all possible Pareto front compositions in the design-space for certain multiple optimization criteria. The general ansatz is to collect as many experimental data on alloy systems as available and develop interpolation and extrapolation models for unknown compositions.

The CALPHAD method (CALculation of PHAse Diagrams, today Computer Coupling of Phase Diagrams and Thermochemistry)[1] allows the prediction of many physical properties of complex multi-component alloys, *e.g.*, phase fractions, phase compositions, or precipitate driving forces at any temperature by using Gibbs free energy databases. Until today, the

M. MARKL, A. MÜLLER, N. RITTER, M. HOFMEISTER, and C. KÖRNER are with the Friedrich-Alexander-Universität Erlangen-Nürnberg, Martensstr. 5, 91058, Erlangen, Germany. Contact e-mail: matthias.markl@fau.de D. NAUJOKS, H. SCHAAR, K. ABRAHAMS, J. FRENZEL, A.P.A. SUBRAMANYAM, A. LUDWIG, J. PFETZING-MICKLICH, T. HAMMERSCHMIDT, R. DRAUTZ, and I. STEINBACH are with the Ruhr-Universität Bochum, Universitätsstr. 150, 44801, Bochum, Germany. R. RETTIG is with the Thermo-Calc Software AB, Råsundavägen 18, 16967, Solna, Sweden. R.F. SINGER is with the Neue Materialien Fürth GmbH, Dr.-Mack-Str. 81, 90762, Fürth, Germany.
Manuscript submitted March 15, 2018.
Article published online June 30, 2018.

improvement of the underlying databases is ongoing, especially in the field of superalloys.[2–4]

Several studies applying various approaches have been published in the field of superalloys. One example is a combinatorial brute-force algorithm for scanning large design-spaces using model characteristics like creep resistance, microstructural stability, castability, density, and cost.[5] Lass applied computational thermodynamics to design a Co-Ni-base superalloy out of six elements avoiding the formation of secondary phases.[6] A mesh adaptive search algorithm in combination with a CALPHAD software is used to determine several design objectives, the optimum alloy compositions, and processing conditions. A further improvement for the optimization of processing conditions, is the integration of the γ'-precipitation kinetics[7] considering higher computational effort for the phase evolution prediction. Another approach is the combination of CALPHAD computations together with artificial neural networks,[8] whereby this approach is only valid within a small parameter variation to well-known alloy compositions. Global optimization techniques together with large experimental databases are applied for designing alloys with optimum composition.[9–11] Promising results are achieved by coupling genetic search algorithms with CALPHAD computations.[9,12,13] Li et al. proposed a computational framework combining genetic algorithms, CALPHAD computations, and mechanistic material models to optimize the alloy composition within the ternary system Ni-Al-Cr.[14] However, the coupling of a genetic algorithm to additional, computationally expensive models, prevent the optimization within a large n-dimensional design-space. Therefore, simplified surrogate models need to be defined,[15] which are easy to couple into a multi-criteria optimization problem.

In this work, the numerical multi-criteria optimization tool MultOpt++ using a genetic search algorithm, CALPHAD calculations, and semi-empirical as well as surrogate models for alloy development is presented. Its successful application for the development of rhenium-free single-crystal Ni-base superalloys ERBO/13[16,17] and ERBO/15[18,19] is revisited. One important goal during the optimization process is the replacement of rhenium by other refractory elements like tungsten and molybdenum. The higher amount of refractory elements may cause phase instability and the evolution of detrimental, brittle topologically close-packed (TCP) phases.[20–22] Since the described optimization procedure does not apply for phase stability of Ni-base superalloys, we present a possible route to develop a surrogate model for integration into the optimization procedure.

II. NUMERICAL APPROACH

The numerical approach in our simulation-assisted alloy development is based on a multi-criteria, multi-start optimization model using sequential quadratic programming described earlier.[16] The semi-empirical equation model for the room-temperature density as well as the model for the temperature-depended misfit by Caron et al.,[23] and the model for solid solution strengthening index I_{SSS} by Fleischmann et al.[24] are applied. Thermodynamic equilibrium material properties are provided by the CALPHAD method. These computations are only applied to a subset of possible compositions and the results are approximated by a Kriging surrogate model.[15,25]

All alloying elements with their concentration range set up the design-space. The probability to find the global optimal composition is increased by choosing various starting points across the whole design-space. Within this space, optimum alloy compositions for certain optimization criteria are searched applying the surrogate and semi-empirical models. The accuracy of the surrogate models is improved by refining the approximation with the current set of optimal compositions before each restart.

A. MultOpt

The first implementation of the optimization tool (termed MultOpt, Matlab-based[16]) uses a single-criterion optimization function, i.e., only one goal can be optimized at a time. However, the optimization of Ni-base superalloys demands multiple optimization goals, e.g., maximizing the solid solution strengthening index and minimizing the density. Accordingly, in this multi-criteria optimization, the solid solution strengthening index is optimized while sampling the density and holding constant during optimization. A final alloy composition is found by further post-processing the Pareto front, i.e., choosing the ideal composition to satisfy additional criteria. This program flow leads to a multi-start, multi-criteria optimization with limited computational effort. However, the method works less well, if more than two criteria are optimized, because each additional criterion increases the number of dimensions of the sampling domain. In addition, the Pareto front contains maximally as many compositions as the number of sampling points for the density. Therefore, an improved optimization routine which allows single-start, simultaneous multi-criteria optimization without limitations on the number of optimization criteria is presented in the present paper.

B. MultOpt++

The new plugin-based structure of the optimization tool MultOpt++ (C++-based) replaces every part of the previous alloy-by-design computational routine and is easily extendable by new features. All property models, surrogate modeling methods, execution modes, starting point selection algorithms, optimization library kernels, and other components are represented by a certain plugin. This allows to combine, for example, models based on different thermodynamic databases or even different CALPHAD applications. It is also possible to apply different optimization algorithms to improve calculation effort or result accuracy.

A simplified schematic representation of the multi-criteria optimization tool for finding the Pareto front is shown in Figure 1.
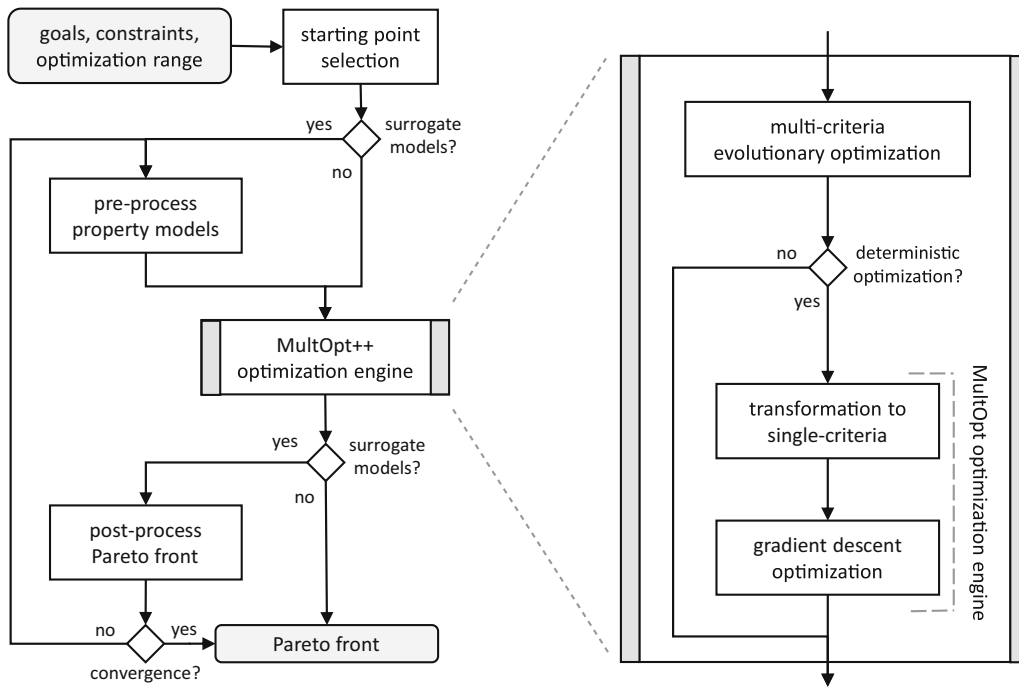
Fig. 1—Schematic representation of the multi-criteria optimization with new evolutionary algorithm-based optimization engine of MultOpt++ software.

It mainly consists of four steps: The selection of appropriate starting points in the design-space, the pre-processing of all surrogate property models, the execution of the optimization engine, and the post-processing of the Pareto front if necessary.

1. Starting point selection

The alloy designer has the possibility to manually select starting points if available or use the latin hypercube sampling for an optimal selection of starting points. The improved latin hypercube sampling[26] provides a better distribution of starting points within *n*-dimensional design-spaces requiring higher computational effort.

2. Pre-process property models

If surrogate property models are applied, they need to be initialized before the first run and improved in each iteration of the optimization routine. The starting points are used for the determination of the initial surrogate models, *i.e.*, the property function is evaluated for all starting points and the interpolation is applied by the Kriging algorithm. In further iterations, the surrogate model is improved by minimizing the maximal predicted model error provided by the Kriging algorithm or the maximal expected improvement factor as proposed by Jones *et al.*[27] The Kriging approximation model is dynamically linked into MultOpt++ as external C-compiled Matlab DACE-toolbox library.[28]

3. Optimization engine

The insights of the MultOpt++ optimization engine are illustrated in Figure 1 (right). As demonstrated by many researches in a wide range of approaches,

evolutionary algorithms are effective for solving multi-objective optimization problems.[29–32] Therefore, the first optimization step is performed by an evolutionary

algorithm provided by the powerful optimization library Geneva "Ivrea - Via Arduino" 1.6.1*. Since evolutionary algorithms typically need many iterations, the last optimization is optionally performed by a deterministic search algorithm. This step requires the transformation of multi-criteria to a single-criterion optimization problem, in a similar way as in MultOpt. The Geneva library provides further probabilistic algorithms as simulated annealing, swarm intelligence, and deterministic algorithms like the gradient descents algorithm. The last one is applied to improve the Pareto front in the last optimization step. Optionally, this step can be combined with one of the other probabilistic search algorithms to benefit from the multi-point start with already Pareto optimal and not random-selected individuals which results in fewer steps with higher computational effort. In the case of optimization with direct usage of objective functions without surrogate models, the Pareto front is the direct result and post-processing as well as multiple optimization runs are skipped.

4. Post-process pareto front

If surrogate models were applied during the optimization run, a post-processing of the Pareto front is necessary. The properties of the predicted optimal compositions have to be recalculated by the direct calculation of the objective functions. For surrogate
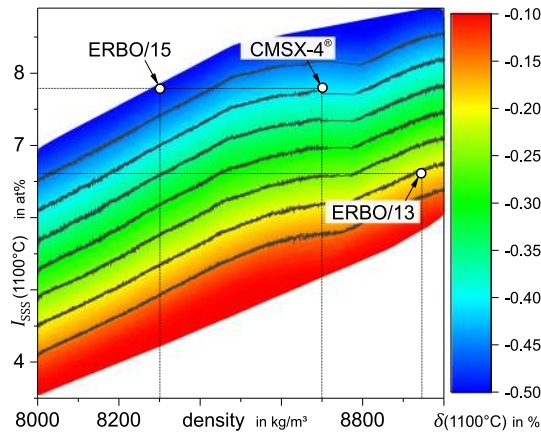
	ERBO/15	ERBO/13	CMSX-4®
Ni	bal. / bal.	bal.	bal.
Al	5.2 / 5.2	4.8	5.6
Co	3.2 / 3.1	8.6	9.6
Cr	6.8 / 6.8	5.0	6.4
Mo	4.2 / 4.2	1.4	0.6
Re	- / -	-	2.9
Ta	- / -	10.1	6.5
Ti	3.3 / 3.3	1.3	1.0
W	8.1 / 7.9	8.8	6.0
	MultOpt++		all values
	/ MultOpt		in wt%

Fig. 2—Optimization of rhenium-free alloys using MultOpt++. Pareto front representing the maximum possible solid solution strengthening index I_{SSS} in dependency of the alloy density and lattice misfit δ at d 1100 °C. The exact constraint on the lattice misfit of -0.2 pct comparable to CMSX-4® causes the high density of the optimal composition ERBO/13. By allowing lower misfits down to -0.5 pct, an optimum composition ERBO/15 was found with a lower density and the same solid solution strengthening index as CMSX-4®. The colored lattice misfit values are only valid for the rhenium-free alloys of the optimization and not for CMSX-4®. Table shows chemical composition (in wt pct, balance is Ni) (Color figure online).

optimization goals, the Pareto selection and for surrogate constraint properties, the feasibility check has to be repeated, respectively. During post-processing, the current Pareto front may worsen and has to be merged with the Pareto front from the previous optimization run. The final optimal points are starting points for the next optimization run also resulting in an improvement of surrogate models within relevant concentration space. If the Pareto front converges, i.e., the optimal values of each single Pareto point cannot be improved within n consecutive optimization runs, the optimization is finished. The number of iterations n is adjustable with a default value of 20.

III. ALLOY DEVELOPMENT REVISITED USING MULTOPT++

The numerical optimization tool MultOpt was already successfully applied in previous studies.[16,18] Starting point was CMSX-4® which is a second-generation single-crystal Ni-base superalloy[33] that is successfully applied in, e.g., aircraft turbines.[34,35] By the addition of 3 wt pct rhenium, a high-temperature creep lifetime is reached due to an extremely low diffusion coefficient. However, the resulting disadvantage is the impossibility of a complete solutionizing and elimination of segregation. More importantly, rhenium is a rare material which is very expensive and prone to speculative manipulation. Therefore, we tried to develop a rhenium-free Ni-base superalloy with similar creep properties as CMSX-4®. The numerical results of previous studies[16,18] are revisited with the modified tool MultOpt++ and presented here.

The basic idea in our previous alloy development effort was as follows. Rhenium as a solid solution strengthener can be replaced by other refractory elements like tungsten and molybdenum. Refractory elements, however, are heavy, i.e., they increase the

density. Tungsten and molybdenum are not as effective as rhenium and one needs higher amounts to account for this, i.e., the density will increase even more. We noticed that certain "control elements" like titanium and tantalum can be used to change the γ/γ' partitioning behavior.[36–39] This means by addition of the control elements, the solid solution strengtheners can be pushed from the γ'-precipitates, where they are less efficient, into the matrix, where they are wanted. With this strategy, alloys with the minimum amount of refractory metals are obtained.

In a first development campaign,[16] we varied mostly tungsten and tantalum and obtained alloy ERBO/13[17] as a result. In our development, we tried to keep γ'-volume fraction and lattice misfit at 1100 °C as close to CMSX-4® as possible. We focused on the partitioning behavior of tungsten during the optimization. In CMSX-4®, tungsten is only slightly enriched in the matrix phase. Therefore, we aimed on an increasing amount to compensate the rhenium effect on creep resistivity. The density, solid solution strengthening index, and lattice misfit of the optimum composition ERBO/13 and the reference CMSX-4® are shown in Figure 2. Calculations are performed using MultOpt++. The second isoline at -0.2 pct lattice misfit shows the Pareto front for the optimization constraints. The solid solution strengthening index of ERBO/13 (6.6 at. pct) is found at 8950 kg/m³. This demonstrates that the current set of strong restrictions prevents achieving the desired index of 7.7 at. pct for CMSX-4®, because densities above 9000 kg/m³ are not desired.

In a second, more successful campaign,[18] we varied molybdenum and titanium and obtained ERBO/15.[19] For ERBO/15, the lattice misfit constraint was somewhat relaxed. Since the main disadvantage of ERBO/13 is the very high density, the strong constraints on the lattice misfit and the γ'-phase fraction are opened to the ranges of -0.5 to -0.1 pct and 43 to 47 mol pct,

respectively. The optimization goals are a minimum density, similar creep resistivity to CMSX-4®, and a rhenium-free alloy composition. The resulting color code of the lattice misfit and the optimal composition ERBO/15 are also shown in Figure 2. The highest solid solution strengthening index can be found for the minimum lattice misfit of -0.5 pct. By choosing the index of CMSX-4®, the optimal composition ERBO/15 with a minimum density of 8300 kg/m^3 is found.

In order to verify our predictions, ERBO/13 as well as ERBO/15 were prepared in the form of small buttons by arc melting and subsequently analyzed regarding physical properties and creep performance.[16,18] Despite weaknesses in the thermodynamic databases, the multi-criteria optimized alloy compositions agree well with most design constraints. This holds true for semi-empirical models (e.g., density or price) as well as thermodynamic properties (e.g., γ'-phase fraction or lattice misfit). Exemplary, the largest mismatch is found for the solid solution strengthening index of ERBO/13, where the experimental determined value is roughly 8 pct lower than the numerical prediction.

Due to a reduced solid solution strengthening index for ERBO/13, its creep resistance is slightly lower than for CMSX-4®. Although ERBO/15 also contains no rhenium, the creep strength is comparable to that of CMSX-4® at low stresses.[18] Therefore, its specific creep strength is even higher due to a significantly reduced density. However, in the high-stress, low-temperature regime CMSX-4® seems superior to both ERBO compositions, which indicates a lower relevance of the solid solution strengthening in contrast to γ'-strengthening.

As an approximation regarding TCP-susceptibility, we used equilibrium calculation with Thermo-Calc engine and database TTNI8 for both alloys.[40] The phase amounts and solvus temperatures of the overall TCP content were compared to CMSX-4® for both alloys. ERBO/13 shows the lowest solvus temperature and TCP-phase amount among these three alloys. ERBO/15, however, shows also a much lower solvus temperature but a higher TCP-phase content at 950 °C and below.

IV. FURTHER OPTIMIZATION OF THE MULTOPT++ APPROACH

The optimization tool MultOpt++ was successfully applied to revisit the alloy development of ERBO/13 and ERBO/15 (see Section III). The improved execution and software structure simplified the optimization procedure, since multiple criteria can be optimized at once. The necessity of dividing additional optimization goals into several single-criteria optimization steps is omitted. Additionally, the plugin-based structure allows easily adopting the routine to new optimization problems and novel property models as well as optimization algorithms. The result of the calculation, i.e., the suggested optimal composition to be tried out in experiment, could be recomputed with minimal variations, e.g., in the cobalt and tungsten contents for ERBO/15 (see Figure 2). Further development of the MultOpt++

tool will focus on important aspects regarding superalloys that are currently neglected (processability or phase stability) or only indirectly accounted for (creep resistance) by the optimization tool. Therefore, we focus within this section on an approach to introduce a surrogate model for phase stability.

Since decades, it is a challenging task to predict the phase instability of Ni-base superalloys causing the formation of TCP-phases. This is due to the fact that the TCP-phase precipitation is a complex time-temperature-depending process of nucleation and growth and during this process different TCP-phases as well as precipitation sequences appear.[21,41,42] The development of phase prediction started with Phase Computation (PHACOMP), based on the electron configuration of the alloying elements.[43] An improvement to this model is new PHACOMP,[44] which is applied in combination with CALPHAD computations until today.[5] Because it suffers from poor and sometimes incorrect predictions, a 2D structure map representation of TCP-phase occurrences is suggested.[45] In addition to the influence of electronic effects,[46] a composition-dependent size factor is introduced to span up the 2D map. These maps are applicable to experimentally observed TCP-phase precipitates in superalloys[47,48] and well suited to validate TCP-phase predictions by combined CALPHAD and phase-field simulations.

Numerical TCP-phase predictions require reliable material databases, a careful simulation setup utilizing thermodynamic computations applying these databases and a final validation, e.g., by structure maps. In the following sections, we describe a crossdisciplinary approach for material database improvements followed by a TCP-phase prediction simulation chain. Finally, we present an idea how to introduce a surrogate model for the TCP-phase prediction applicable in the numerical optimization procedure.

A. Crossdisciplinary Material Database Improvement

More knowledge on TCP-phase formation in binary and ternary systems is necessary to extrapolate correctly to higher order systems. Current research connects combinatorial thin-film experimentation and bulk experimentation with ab-initio simulations to predict TCP-phases in ternary systems.[4] These results are used to improve existing material databases and thereby improve the predictions on the full alloy composition.

In the following, the concept of Crossdisciplinary Material Database Improvement (CMDI) is explained by a general workflow schematic in Figure 3. Starting point is an external input from existing databases or calculations (dotted arrows). This input can for instance be an interesting, yet unknown or not well-known ternary system or composition range in which TCP-phases are expected. Based on this initial input, a thin-film material library of the interesting composition rage will be fabricated on a 100mm diameter substrate by magnetron sputtering using a wedge-type multi-layer approach.[49,50] The material library is annealed and analyzed by energy dispersive X-ray spectroscopy
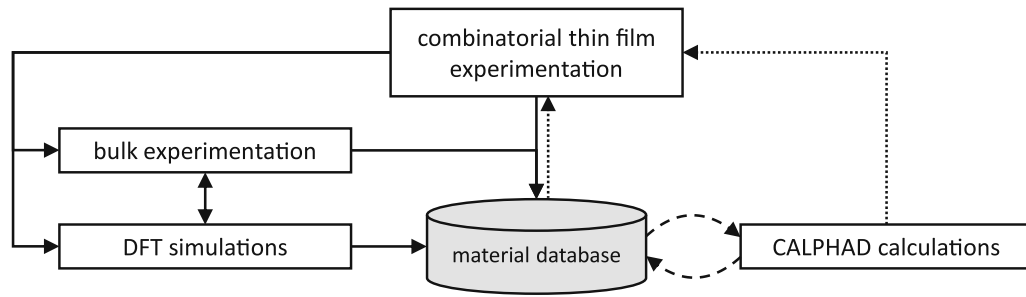
Fig. 3—Schematic workflow of the CMDI approach realized by combining combinatorial thin-film experimentation, bulk experimentation, DFT calculations, as well as CALPHAD calculations.

(EDX), electric resistance measurements, and X-ray diffraction (XRD). The results of the combinatorial thin-film experimentation are direct inputs for the bulk experimentation and arising questions are addressed by *ab-initio* density-functional theory (DFT) calculations. Compositions found to be of interest in the material library are systematized in bulk by arc melting[51,52] and analyzed by scanning electron microscope (SEM), EDX, transmission electron microscope (TEM), and nanoindentation as well. Structural stability and formation energy for the phases found in the material library are analyzed by DFT calculations.[53] DFT calculations and bulk experimentation also exchange their results for further refinement. The combination of all three disciplines (combining combinatorial thin-film experimentation, bulk experimentation, and DFT calculations) enables a better understanding of each of the results on its own but also contribute as experimental/calculated data input to the material database. The updated material database can be used to predict phase diagrams by CALPHAD.[54] The CALPHAD results are crosschecked with the existing experimental data in the library enabling a feedback loop to further refine the CALPHAD predictions (dashed arrows). Figure 4 shows a summary of results from a recent study on the Co-Ti-W system that applied the concept of CMDI.[4] In Figure 4(a), an isothermal section of a ternary phase diagram for the Co-Ti-W system predicted by CALPHAD based on the existing database TCNi8 is shown. Since experimental results as well as DFT calculations indicate the presence of titanium in the μ-phase, a solubility of titanium is modeled by a preliminary modification of the thermodynamic database. Figure 4(b) represents an isothermal section of a ternary phase diagram for the Co-Ti-W system predicted by CALPHAD based on the improved TCNi8 database. Due to the stabilizing effect of titanium that was taken into account in the second simulation, the single-phase region of the μ-phase was enlarged into the ternary (up to approx. 8 at. pct titanium) also the existence range of the μ-phase in the ternary Co-Ti-W system was enlarged. By this, also the expected volume fraction of the μ-phase in the multi-phase regions increased. These results demonstrate the suitability of the CMDI approach to advantageously modify material databases.

B. *TCP-phase Prediction*

Second and higher generation Ni-base superalloys are highly alloyed with refractory elements like tungsten, molybdenum, rhenium, and ruthenium, respectively, to obtain excellent solid solution strengthening and creep properties.[16,18,37,55,56] They solidify in a dendritic microstructure causing microsegregation of alloying elements, low melting eutectic phases, and unfavorably shaped γ'-precipitates.[57–59] An initial solution heat treatment is normally applied to remove microsegregations and eutectic phases and to dissolve the γ'-precipitates followed by further heat treatment steps to ensure well-defined cubic γ'-precipitates.[60,61] A full homogenization heat treatment of these elements in reasonable times is prevented due to a low diffusivity in combination with a preferred segregation into the dendrite cores during solidification.[60,62,63] The remaining segregation of refractory elements in the dendrite cores after heat treatment causes the formation of intermetallic phases (TCP) under service conditions.[64] In Ni-base superalloys, several brittle TCP-phases like σ-, μ-, P-, and R-phases were found,[20–22] which additionally deplete the solid solution strengtheners from the γ-matrix.[65] Experimental investigations showed that nucleation occurs mainly on grain boundaries or on a previously formed metastable σ-phase within the γ-region.[42,65] The morphologies are various, *e.g.*, plate-like, lath-type, or globular[22,66] with a preferred directional growth and coherency with {111}γ or {100}γ planes.[20–22] The embrittlement under load due to TCP-phases in combination with a surrounding matrix of depleted alloying elements results in degraded mechanical as well as chemical properties.[37,42]

In order to minimize TCP-phase formation in newly developed Ni-base superalloys, the numerical optimization tool needs to be extended by a TCP-phase prediction model. Since the evolution of TCP-phases is influenced by manufacturing and service conditions, a comprehensive numerical simulation is necessary, which is illustrated in Figure 5. The casting parameters are used to predict the primary dendritic arm spacing (PDAS). All further simulation steps make use of thermodynamic material databases according to the superalloy base material. Here, the improved material databases by the CMDI approach described in Section IV–A are necessary to ensure a more reliable
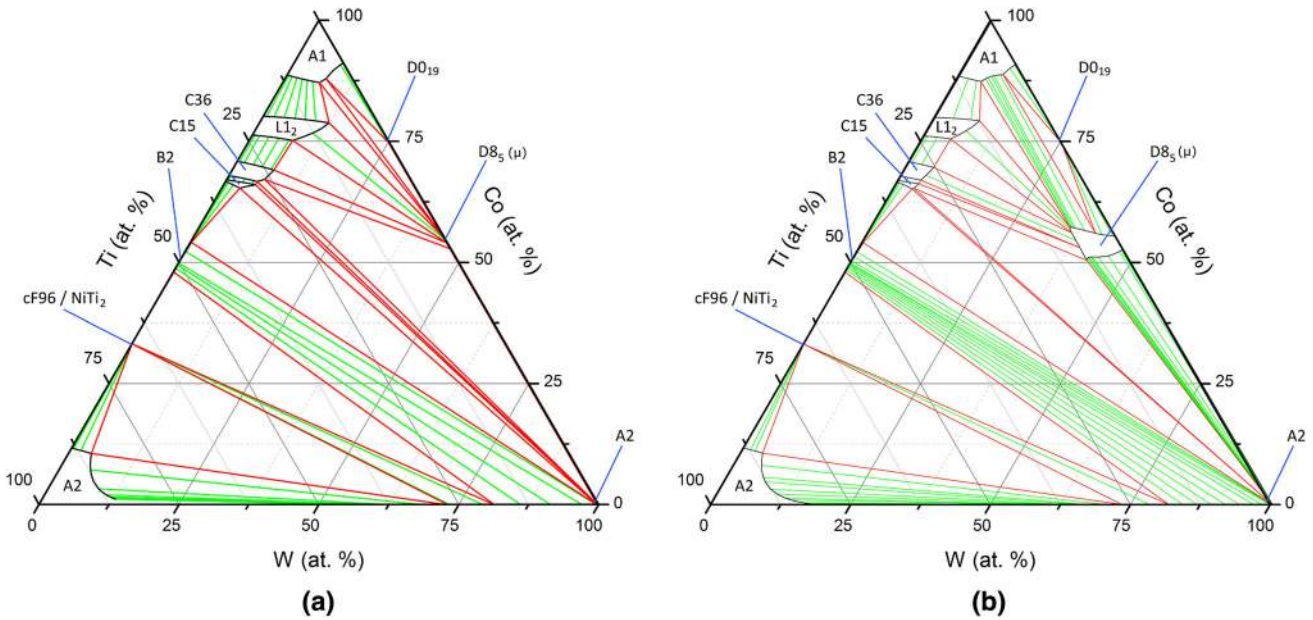
Fig. 4—Current (a) and improved (b) isothermal sections of a ternary phase diagram for the Co-Ti-W system predicted by CALPHAD. Applying the CDMI approach the enlarged μ-phase was detected. Adapted from Ref. [4], with permission (Color figure online).
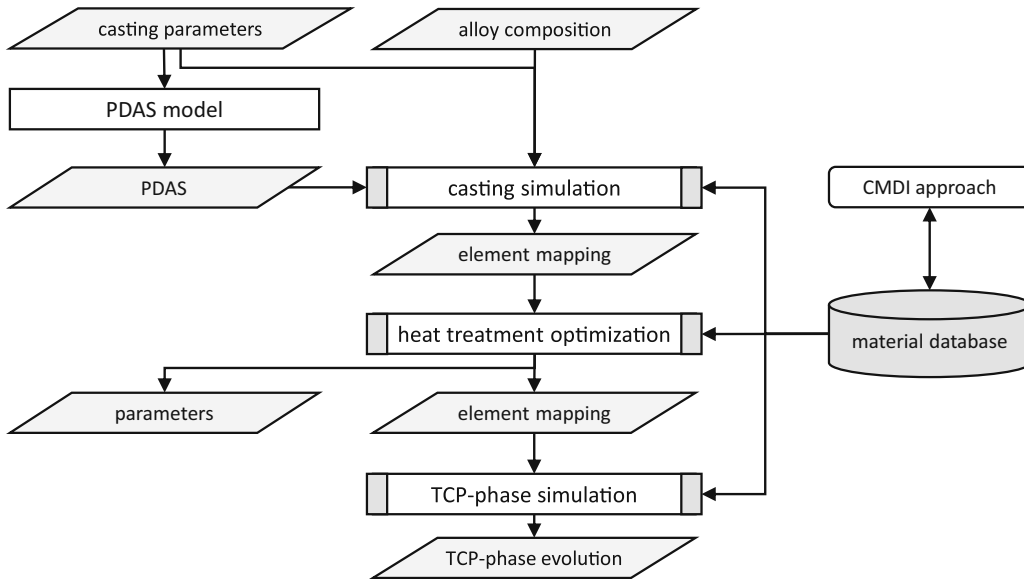

Fig. 5—Overview of TCP simulation chain: estimation of PDAS λ followed by the simulation of the solidification during the casting process, heat treatment, and TCP-phase formation. All simulations can make use of improved material databases by the CMDI approach.

prediction of the whole simulation chain. The solidification simulation is a phase-field simulation which is initialized with the primary dendrite arm spacing and the alloy composition.[67] The result is a segregation profile which is the input for an optimization tool to predict the best heat treatment parameters to maximize homogeneity.[68] The resuming segregation profile after heat treatment is finally applied for phase-field simulations to predict microstructural evolution of γ/γ' considering the influence of multi-component diffusion on nucleation and growth of TCP-phases. Once the whole simulation chain is established and validated, it is possible to extract information regarding designing, processing, and material properties of the studied alloy composition. Here, we only focus on the last result of the TCP-phase evolution, which is finally converted into a surrogate model for the application in the optimization tool MultOpt++.

1. PDAS model

The casting parameters are determined by our new investment casting process named Fluidized Carbon Bed Cooling (FCBC).[69] Compared to the well-known liquid-metal cooling (LMC) process,[70–72] FCBC applies

an inert gas fluidized bed of glassy carbon beads instead of a bath of molten tin to carry a buoyant layer of freely movable insulation particles.[73] The so-called Dynamic Baffle[74] properly separates the heating and solidification zones as it perfectly adapts the contour of the solidifying component at any time during withdrawal. The low-density Dynamic Baffle material is, similar to the bed material, based on carbon. The Dynamic Baffle is crucial to improve the temperature gradient in investment casting. Dynamic Baffle, carbon's superalloy material compatibility and innovative process control over previous fluidized bed attempts are key features in the robust FCBC approach.[69]

Because the FCBC process achieves higher temperature gradients, increased withdrawal rates in comparison to conventional investment casting devices are possible. The resulting PDAS is predicted by the empirical model $\lambda = K \times G^{-0.5} \times v^{-0.25}$,[75] where K is a constant (1444 for Ni-base superalloys[76]), G is the temperature gradient, and v is the solidification velocity. In the case of directional solidification casting, the solidification velocity is approximated by the withdrawal rate. The temperature gradient G for a certain FCBC process setup can either be determined by numerical simulation[77] or by one sample experiment including the measurement of the PDAS.[69] The lowest PDAS around 300 μm for a single-crystal microstructure is achieved for a withdrawal rate of 5.0mm/min. This reduction to the industrial state of the art (larger 400 μm for the geometry studied) significantly reduces element segregation and heat treatment durations.[62,78,79]

2. Casting simulation

The objective of the next step in the simulation chain is to understand the formation of the as-cast microstructure which represents a starting point for subsequent heat treatment simulations. The numerical approach relies solely on the input of the casting parameters, the nominal alloy composition, and the estimated PDAS. The final output are concentration maps of all alloying elements.

As modeling approach, the multi-component multi-phase-field model[80,81] is applied. The free energy formulation of the system serves as basis considering contributions of the interfacial, chemical, and elastic energy. Following several mathematical operations[82] and the use of the double-obstacle potential, the phase-field equation can be formulated in antisymmetric approximation

$$\dot{\phi}_\alpha = \sum_{\beta=1,...,N} M_{\alpha\beta} \left\{ \sigma_{\alpha\beta} \left[\phi_\beta \nabla^2 \phi_\alpha - \phi_\alpha \nabla^2 \phi_\beta + \frac{\pi^2}{2\eta^2}(\phi_\alpha - \phi_\beta) \right] + \frac{\phi}{\eta}\sqrt{\phi_\alpha \phi_\beta} \underline{\Delta g_{\alpha\beta}} \right\} \qquad \sum_{\alpha=1,...,N} \phi_\alpha = 1,$$

where $M_{\alpha\beta}$ represents the interface mobility, $\sigma_{\alpha\beta}$ the interface energy, η the interface width, and $\Delta g_{\alpha\beta}$ the Gibbs free energy difference between the phases α and β. Basically, ϕ_α is an indicator function used for tracking the moving interface during the process of solidification

with values between 0 (solid bulk) and 1 (liquid melt). The contribution of the Gibbs free energy is evaluated by coupling to the software package Thermo-Calc. As a result, an optimal thermodynamic description of the solute partitioning in the system during the solidification process is ensured. Diffusion is solved with respect to all elements of the alloy composition. The amount of phases is limited to liquid, γ and primary γ'.

The presented numerical approach for solidification during casting is validated by experimental results of directionally solidified CMSX-4® applying the vertical Bridgman process.[83] As software tool, the commercial software MICRESS® in combination with the databases TCNI8 and MOBNI4 is used. The thermal gradient is taken from previous work,[83] where this value has been determined by a combined numerical and experimental approach. In the model, the same withdrawal rates are considered as in the case of solidification experiments. The PDAS is taken as input for the simulations.

In Figure 6, the concentration distributions for rhenium and aluminum gained by simulations (a, b) and experiments (c,d) are presented, respectively. The experimental concentration maps were determined by electron microprobe analysis (EMPA).[84] For both elements, a good agreement between the simulated and the experimentally gained concentration distributions can be observed, e.g., the rhenium concentration in the center of the dendrite is 4.5 wt pct (a) and 4.9 wt pct (b), respectively. We note that the experimentally determined composition of γ' in the interdendritic regions lies significantly below the theoretical equilibrium composition, which is probably due to the size of the electron beam which averages γ and γ' regions.

3. Heat treatment optimization

The goal during solution heat treatment is to achieve the highest diffusion coefficients by a maximum temperature profile while avoiding incipient melting in order to prevent diminishing the mechanical properties.[85–87] The time-consuming experimental approach to define the solution heat treatment by measuring incipient melting temperatures for different heating rates by differential scanning calorimetry[88] is circumvented by a numerical heat treatment optimization procedure.[68] The computed heat treatment needs an experimental validation, because incipient melting temperature estimation errors in the range of ± 20 K depending on the alloy composition may occur due to inaccuracies in the material databases.

The original optimization procedure consists of three steps: pre-processing of experimentally measured the as-cast concentration fields into a numerical representation, optimization of solution heat treatment, and the prediction of a corresponding process window. The pre-processing step is mainly redundant once the procedure is integrated in our simulation chain since numerically predicted concentration fields are already available from the casting simulations. During heat treatment optimization, the maximum stepwise temperature history is determined without incipient melting. The phase-field model applied for heat treatment is a
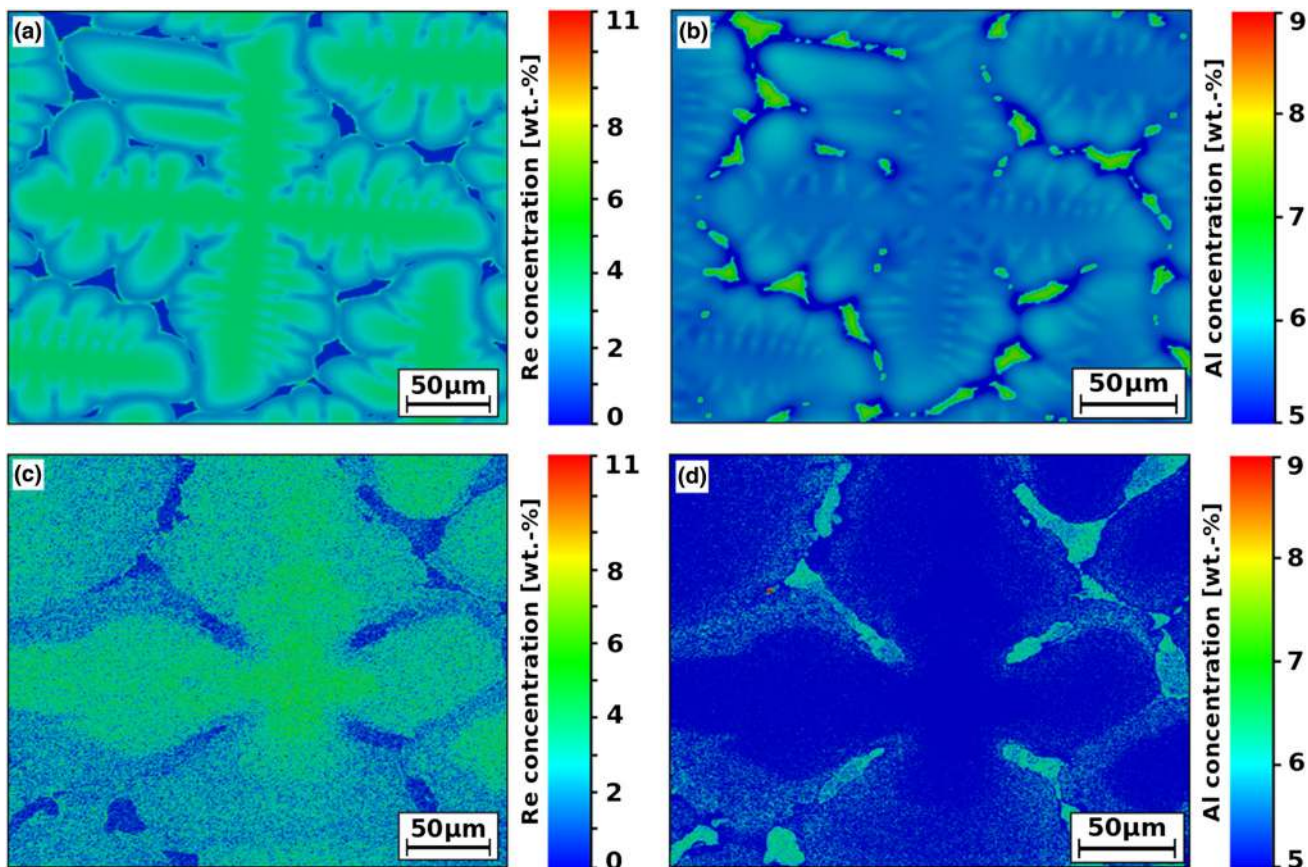
Fig. 6—Comparison of simulated results and experimental measurements (vertical Bridgman process sample measured by EMPA) for the concentration distribution of rhenium (*a*, *c*) and aluminum (*b*, *d*) in CMSX-4®, respectively (Color figure online).

diffuse-interface approach,[81] which requires similarly to the casting model the interface energy and mobility. The software tool MICRESS® is applied using thermodynamic and kinetic databases.[68] Since processing restrictions sometimes hinder applying maximum temperatures, a process window with lowered maximum temperatures is computed. The final results of the simulation are the concentration fields for all elements of the alloy composition after the optimal heat treatment.

A comparison between microprobe measurements of commercially purchased single-crystal plates and simulation results of the chromium segregation in CMSX-4® in the as-cast state and after heat treatment is shown in Figure 7. The microprobe measurements (a) are pre-processed to get a numerical representation of the chromium concentrations (b). A well accordance between the homogenized states in the experimental and numerical results after heat treatment is reached, (c) and (d), respectively.

4. *TCP-phase simulation*

One approach to approximate TCP-phase susceptibility is the application of equilibrium calculations with Thermo-Calc, as mentioned in Section III. The TCP-phase precipitation model is based on the Kampmann–Wagner binary system method and was extended by Rettig *et al.*[40] for multi-component systems. On

every time step, the nucleation rate and precipitation growth are evaluated. The nucleation rate depends on the free enthalpy of nucleation, which is calculated using the CALPHAD method. The precipitation growth includes the thermodynamic equilibrium for the chemical potential of precipitate and the matrix interface as well as the flux balance for each element. A detailed model description as well as simulation results are presented in Reference 40 and validated in Reference 18.

This approach, as well as other existing models to predict precipitation on TCP-phases are mainly based on simple models, *e.g.*, by using precipitate classes without full-field resolution of the concentration fields.[89,90] The complex behavior of TCP-phases in γ/γ' taking into account the microstructural evolution, diffusion processes, available nucleation sites, interface energies, and the interaction between TCP-phases is an ongoing research topic. All these aspects can be combined in phase-field simulations[82,91,92] and then applied to TCP-phase precipitation in Ni-base superalloys.

5. *TCP surrogate model*

Due to the high computational effort, it is not possible to include the whole TCP-phase precipitation simulation chain into the optimization routine for the design of complex Ni-base superalloys. Therefore, the main idea is the approximation with a surrogate model, which is coupled into the optimization procedure within the
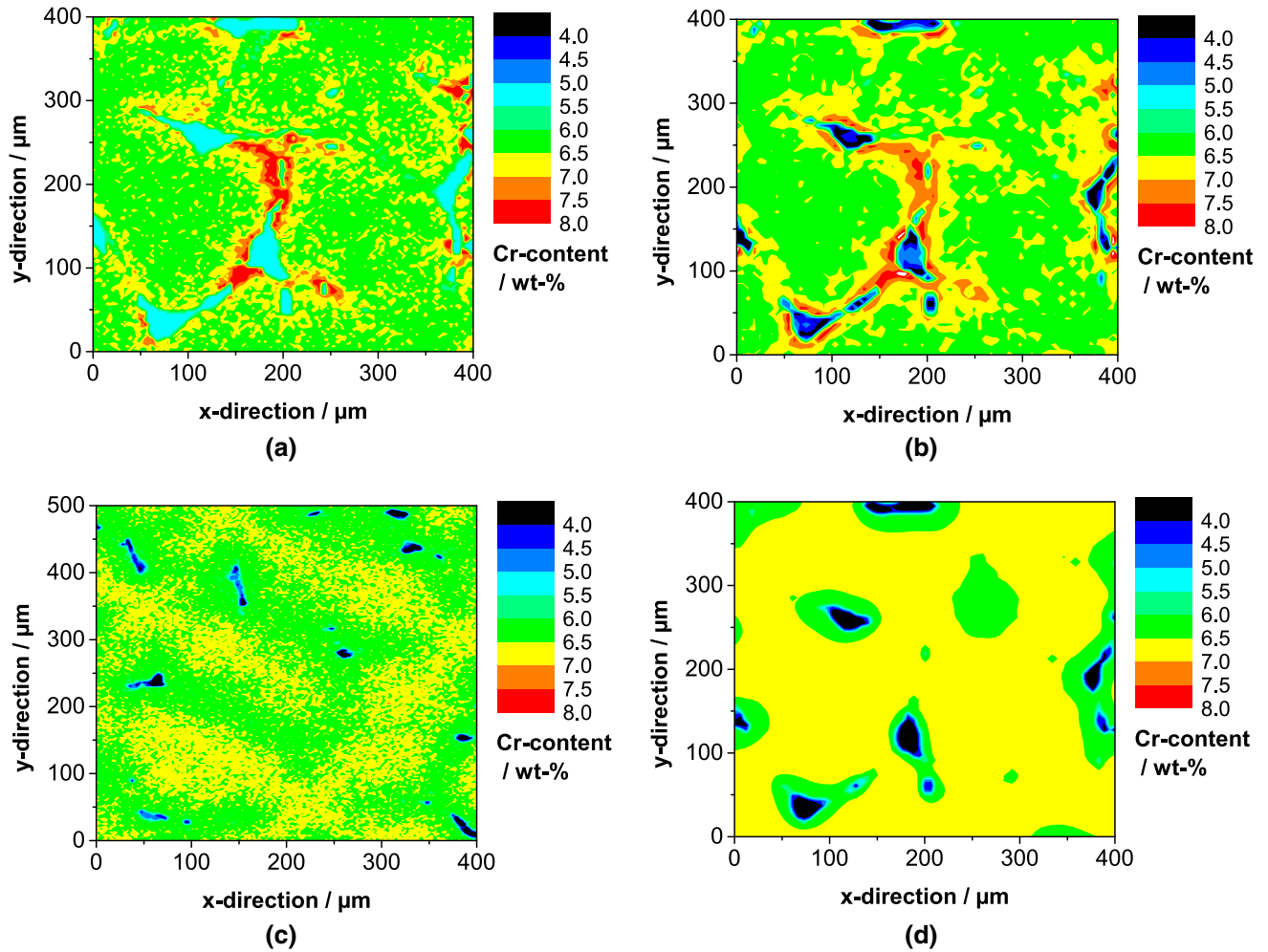
Fig. 7—Comparison of the chromium segregation of CMSX-4® measured by microprobe of purchased single-crystal plates (*a*, *c*) and simulated by phase-field simulation (*b*, *d*). Shown are the as-cast states (*a*, *b*), and the states after heating up and holding at 1573 K (1300 °C) for 1 h (*c*, *d*). Reprinted from Ref. [68], with permission (Color figure online).

"pre-process property models" step (Figure 1). This approach has two necessary prerequisites. First, each simulation tool and subsequently its combination into the simulation chain needs to be validated by well-known reference alloy compositions like CMSX-4®. Second, a widespread numerical sensitivity analysis on the simulation chain on a large design-space needs to be executed to develop a regression-based model covering the most important findings.

Our current approach for the development of a regression-based model bases on the Johnson–Mehl–Avrami equation[93] for the time-dependent transformation of nuclei

$$f_V(t, c, T) = f_V^{eq}(c, T)\left[1 - \exp\left(-k(c, T) \cdot t^{n(c,T)}\right)\right],$$

where $f_V(t, c, T)$ is the time-dependent fraction of the sum of all TCP-phases and $f_V^{eq}(c, T)$ is the TCP-phase amount provided by thermodynamic equilibrium CALPHAD calculations. The Avrami coefficients k and n are assumed to be dependent on the concentration c and

temperature T and are to be derived. Although, the evolution of different types of TCP-phases is much more complex with nucleation and growth in parallel as well as phase transformation, this approach is well suited to model the overall time evolution.[18] The predictive power of this surrogate model is defined by the exact determination of these parameters, which have to be evaluated by the regression analysis. Once all individual simulation tools of the simulation chain are completely validated, the regression analysis of TCP-phase predictions from the whole simulation chain is the next research step.

V. SUMMARY

In this paper, we present a numerical model which was applied to revisit the development of different Ni-base superalloys and describe a numerical approach to predict the formation of TCP-phases for further inclusion into the optimization procedure by a surrogate model:

1. A single-start multi-criteria optimization tool MultOpt++ based on a multi-start derivative is presented. The simple extension to further (surrogate) models due to its plugin structure, the application of multiple optimization goals, and an improved post-processing of the Pareto front is demonstrated.
2. The development of ERBO/13 and ERBO/15 is revisited and the achievements as well as the optimization weaknesses are discussed. Although, models on important topics like TCP-phase formation are not applied, a set of newly designed and highly promising alloy compositions was found.
3. A possible model extension for the multi-criteria optimization regarding phase stability is presented. The whole simulation chain combines different numerical tools to finally predict the evolution of TCP-phases. A development ansatz for a surrogate model is presented including the coupling to the multi-criteria optimization tool MultOpt++. Besides the information on TCP-phase formation, the simulation chain offers the possibility for further surrogate models regarding designing, processing, and material properties of Ni-base superalloys. These improvements may help to find better rhenium-free alloy compositions with properties more close to or even better as the performance of CMSX-4®.

REFERENCES

1. B. Sundman, B. Jansson, and J.-O. Andersson: *CALPHAD*, 1985, vol. 9, pp. 153–90.
2. N. Dupin and B. Sundman: *Scand. J. Metall.*, 2001, vol. 30, pp. 184–92.
3. J. Bratberg, H. Mao, L. Kjellqvist, A. Engström, P. Mason, and Q. Chen: *Proc. Int. Symp. Superalloys, 12th*, 2012, pp. 803–12.
4. D. Naujoks, Y. Eggeler, P. Hallensleben, J. Frenzel, S. Fries, M. Palumbo, J. Koßmann, T. Hammerschmidt, J. Pfetzing-Micklich, G. Eggeler, and E. Spiecker: *Acta Mater.*, 2017, vol. 138, pp. 100–10.
5. R. Reed: *Acta Mater.*, 2009, vol. 57, pp. 5898–5913.
6. E.A. Lass: *Mater. Trans. A*, 2017, vol. 48, pp. 2443–59.
7. N. Saunders, M. Fahrmann, and C. Small: *Proc. Int. Symp. Superalloys, 9th*, 2000, pp. 803–11.
8. D.J. Crudden, B. Raeisinia, N. Warnken, and R.C. Reed: *Mater. Trans. A*, 2013, vol. 44, pp. 2418–30.
9. F. Tancret: *Modell. Simul. Mater. Sci. Eng.*, 2012, vol. 20, Art. No. 045012.
10. I. Egorov-Yegorov and G. Dulikravich: *Manuf. Process.*, 2005, vol. 20, pp. 569–90.
11. Y. Shmotin, A. Logunov, D. Danilov, and I. Leshchenkoi: *MATEC Web Conf.*, 2014, vol. 14, Art. No. 17005.
12. F. Tancret: *Modell. Simul. Mater. Sci. Eng.*, 2013, vol. 21, Art. No. 045013.
13. E. Menou, G. Ramstein, E. Bertrand, and F. Tancret: *Modell. Simul. Mater. Sci. Eng.*, 2016, vol. 24, Art. No. 055001.
14. S. Li, U. Kattner, and C. Campbell: *Integr. Mater. Manuf. Innov.*, 2017, vol. 6, pp. 229–48.
15. R. Rettig and R. Singer: *Modell. Simul. Mater. Sci. Eng.*, 2014, vol. 22, Art. No. 085002.
16. R. Rettig, N. Ritter, H. Helmer, S. Neumeier, and R. Singer: *Modell. Simul. Mater. Sci. Eng.*, 2015, vol. 23, Art. No. 035004.
17. R. Rettig, R. Singer, H. Helmer, and S. Neumeier: *EP2725110A1: Kriechbestndige, rheniumfreie Nickelbasissuperlegierung*, 2012.
18. R. Rettig, K. Matuszewski, A. Müller, H. Helmer, N. Ritter, and R. Singer: *Proc. Int. Symp. Superalloys, 13th*, 2016, pp. 35–44.
19. T. Göhler, R. Rettig, R. Singer, S. Neumeier, and N. Ritter: *EP3091095A1: Rheniumfreie Nickelbasis-Superlegierung mit niedriger Dichte*, 2015.
20. R. Darolia, D. Lahrman, and R. Field: *Proc. Int. Symp. Superalloys, 6th*, 1988, pp. 255–64.
21. C. Rae, and R. Reed: *Acta Mater.*, 2001, vol. 49, pp. 4113–25.
22. B. Dubiel, P. Indyka, T. Moskalewicz, A. Kruk, M. Zubko, I. Kalemba-Rec, and K. Berent: *J. Microsc.*, 2017, vol. 266, pp. 239–48.
23. P. Caron: *Proc. Int. Symp. Superalloys, 9th*, 2000, pp. 737–46.
24. E. Fleischmann and M. Miller: *Acta Mater.*, 2015, vol. 87, pp. 350–56.
25. D. Krige: *J. Chem., Metall. Min. Soc. S. Afr.*, 1951, vol. 52, pp. 119–39.
26. B. Beachkofski and R. Grandhi: *American Institute of Aeronautics and Astronautics Paper*, 2002, pp. 1247–81.
27. D. Jones: *J. Global Optim.*, 1998, vol. 13, pp. 455–92.
28. S. Lophaven, H. Nielsen and J. Søndergaard: *A MATLAB Kriging Toolbox*, Informatics and Mathematical Modelling, Technical University of Denmark, DTU, 2002.
29. E. Zitzler, K. Deb, and L. Thiele: *Evol. Comput.*, 2000, vol. 8, pp. 173–95.
30. J. Reddy and N. Kumar: *Water Resour. Manag.*, 2006, vol. 20, pp. 861–78.
31. C. Coello: *Comput. Method. Appl. M*, 2002, vol. 191, pp. 1245–87.
32. P. Limbourg: *Evolutionary Multi-Criterion Optimization, 3rd*, 2005, pp. 413–27.
33. K. Harris, G. Erickson, S. Sikkenga, W. Brentnall, J. Aurrecoechea, and K. Kubarych: *Proc. Int. Symp. Superalloys, 7th*, 1992, pp. 297–306.
34. K. Fullagar, R. Broomfield, M. Hulands, K. Harris, G. Erickson, and S. Sikkenga: *J. Eng. Gas Turbines Power*, 1996, vol. 118, pp. 380–88.
35. R. Broomfield, D. Ford, J. Bhangu, M. Thomas, D. Frasier, P. Burkholder, K. Harris, G. Erickson, and J. Wahl: *J. Eng. Gas Turbines Power*, 1998, vol. 120, pp. 595–608.
36. Y. Amouyal, Z. Mao, and D. Seidman: *Acta Mater.*, 2010, vol. 58, pp. 5898–5911.
37. A. Heckl, S. Neumeier, M. Göken, and R. Singer: *Mater. Sci. Eng. A*, 2011, vol. 528, pp. 3435–44.

38. M. Pröbstle, S. Neumeier, P. Feldner, R. Rettig, H. Helmer, R. Singer, and M. Göken: *Mater. Sci. Eng. A*, 2016, vol. 676, pp. 411–20.
39. N. Ritter, E. Schesler, A. Müller, R. Rettig, C. Körner and R. Singer: *Adv. Eng. Mater.*, 2017, vol. 19, Art. No. 1700150.
40. R. Rettig and R. Singer: *Acta Mater.*, 2011, vol. 59, pp. 317–27.
41. K. Matuszewski, A. Müller, N. Ritter, R. Rettig, K. Kurzydowskiand, and R. Singer: *Adv. Eng. Mater.*, 2015, vol. 17, pp. 1127–33.
42. K. Matuszewski, N. Ritter, H. Matysiak, Z. Peng, I. Povstugar, P. Choi, J. Müller, D. Raabe, E. Spiecker, K. Kurzydowski, and R. Singer: *Acta Mater.*, 2015, vol. 95, pp. 274–83.
43. W. Boesch and J. Slaney: *Met. Prog.*, 1964, vol. 86, pp. 109–11.
44. M. Morinaga, N. Yukawa, H. Adachi and H. Ezaki: *Proc. Int. Symp. Superalloys*, 5th, 1984, pp. 523–32.
45. B. Seiser, R. Drautz, and D. Pettifor: *Acta Mater.*, 2011, vol. 59, pp. 749–63.
46. B. Seiser, T. Hammerschmidt, A. Kolmogorov, R. Drautz, and D. Pettifor: *Phys. Rev. B*, 2011, vol. 83, Art. No. 224116.
47. J. Koßmann, C.H. Zenk, I. Lopez-Galilea, S. Neumeier, A. Kostka, S. Huth, W. Theisen, M. Göken, R. Drautz, and T. Hammerschmidt: *J. Mater. Sci.*, 2015, vol. 50, pp. 6329–38.
48. I. Lopez-Galilea, J. Koßmann, A. Kostka, R. Drautz, L. Mujica Roncery, T Hammerschmidt, S. Huth, and W. Theisen: *J. Mater. Sci.*, 2016, vol. 51, pp. 2653–64.
49. A. Janghorban, J. Pfetzing-Micklich, J. Frenzel, and A. Ludwig: *Adv. Eng. Mater.*, 2014, vol. 16, pp. 588–93.
50. A. Ludwig, R. Zarnetta, S. Hamann, A. Savan, and S. Thienhaus: *Int. J. Mater. Res.*, 2008, vol. 99, pp. 1144–49.
51. J. Frenzel, E. George, A. Dlouhy, C. Somsen, M. Wagner, and G. Eggeler: *Acta Mater.*, 2010, vol. 58, pp. 3444–58.
52. J. Frenzel, A. Wieczorek, I. Opahle, B. Maaß, R. Drautz, and G. Eggeler: *Acta Mater.*, 2015, vol. 90, pp. 213–31.
53. T. Hammerschmidt, A. Bialon, D. Pettifor and R. Drautz: *New J. Phys.*, 2013, vol. 15, art. 115016.
54. H. Lukas, S. Fries, and B. Sundman: *Computational Thermodynamics: The Calphad Method*, Cambridge University Press, Cambridge, 2007, pp. 1–313.
55. H. Harada: *Int. Gas Turbine Congress (Tokyo)*, 2003.
56. R. MacKay, T. Gabb, J. Smialek, and M. Nathal: *JOM*, 2010, vol. 62, pp. 48–54.
57. A. Heckl, R. Rettig, S. Cenanovic, M. Göken, and R. Singer: *J. Cryst. Growth*, 2010, vol. 312, pp. 2137–44.
58. G. Fuchs and B. Boutwell: *Mater. Sci. Eng. A*, 2002, vol. 333, pp. 72–79.
59. M. Karunaratne, D. Cox and P. Carter: *Proc. Int. Symp. Superalloys, 9th*, 2000, pp. 263–72.
60. G. Fuchs: *Mater. Sci. Eng. A*, 2001, vol. 300, pp. 52–60.
61. B. Wilson, J. Hickman, and G. Fuchs: *JOM*, 2003, vol. 55, pp. 35–40.
62. M. Lamm, A. Volek, O. Lsebrink, and R. Singer: *Mater. Adv. Power Eng. 2006: Part I*, 2006, vol. 2006, pp. 334–44.
63. M. Karunaratne, C. Rae, and R. Reed: *Metall. Mater. Trans. A*, 2001, vol. 32, pp. 2409–21.
64. A. Volek, and R. Singer: *Proc. Int. Symp. Superalloys, 10th*, 2004, pp. 713–18.
65. J. Liu, J. Li, F. Hage, P. Ghosh, J. Li, W. Wang, Z. Chen, T. Wang, W. Tang, Q. Ramasse, and P. Schumacher: *Acta Mater.*, 2017, vol. 131, pp. 169–86.
66. K. Cheng, C. Jo, T. Jin, and Z. Hu: *J. Alloys Compd.*, 2011, vol. 509, pp. 7078–86.
67. I. Lopez-Galilea, S. Huth, S. Fries, N. Warnken, I. Steinbach, and W. Theisen: *Metall. Mater. Trans. A*, 2012, vol. 43, pp. 5153–64.
68. R. Rettig, N. Ritter, F. Müller, M. Franke, and R. Singer: *Metall. Mater. Trans. A*, 2015, vol. 46, pp. 5842–55.
69. M. Hofmeister, M. Franke, C. Koerner, and R. Singer: *Metall. Mater. Trans. B*, 2017, vol. 48, pp. 3132–42.
70. A. Giamei and J. Tschinkel: *Metall. Trans. A*, 1976, vol. 7, pp. 1427–34.
71. A. Lohmüller, W. Eßer, J. Großmann, M. Hördler, and J. Preuhs: *Proc. Int. Symp. Superalloys*, 9th, 2000, pp. 181–88.
72. A. Elliott, S. Tin, W. King, S.-C. Huang, M. Gigliotti, and T. Pollock: *Metall. Mater. Trans. A*, 2004, vol. 35A, pp. 3221–31.
73. M. Hofmeister, K. Wirth, and R. Singer: *DE102014216766: Verfahren zur Herstellung eines Gussbauteils*, 2014.
74. R. Singer, T. Fitzgerald, and P. Krug: *WO9605006: Method and Device for Directionally Solidifying a Melt*, 1995.
75. W. Kurz and D. Fisher: *Fundamentals of Solidification*, 3rd ed., Trans Tech Publications, Zurich, 1989.
76. P. Krug: *Einfluss einer Flüssigmetallkuhlung auf die Mikrostruktur gerichtet erstarrter Superlegierungen*. Ph.D. Thesis, Friedrich-Alexander-Universität Erlangen-Nürnberg, 1998.
77. M. Franke, R. Hilbinger, A. Lohmüller, and R. Singer: *J. Mater. Process. Technol.*, 2013, vol. 213, pp. 2081–88.
78. S. Steuer, P. Villechaise, T. Pollock, and J. Cormier: *Sci. Eng. A*, 2015, vol. 645, pp. 109–15.
79. J. Großmann, J. Preuhs, W. Esser and R. Singer: *Proc. Int. Symp. Liq. Met. Process. Cast.*, 1999, pp. 31–40.
80. J. Eiken, B. Boettger and I. Steinbach: *Phys. Rev. E*, 2006, vol. 73.
81. I. Steinbach, F. Pezzolla, B. Nestler, M. Seeßelberg, R. Prieler, G. Schmitz, and J. Rezende: *Phys. D*, 1996, vol. 94, pp. 135–47.
82. I. Steinbach: *Modell. Simul. Mater. Sci. Eng.*, 2009, vol. 17, Art. No. 073001.
83. P. Hallensleben, H. Schaar, P. Thome, N. Joens, A. Jafarizadeh, I. Steinbach, G. Eggeler, and J. Frenzel: *Mater. Des.*, 2017, vol. 128, pp. 98–111.
84. P. Hallensleben: *Werkstoffwissenschaftliche Untersuchungen zur Entwicklung von Mikrostrukturen und Defekten bei der einkristallinen erstarrung von Nickelbasis-Superlegierungen mittels einer bridgman-seed-technik*, Bochum, 2017.
85. K. Gasko, G. Janowski, and B. Pletka: *Mater. Sci. Eng.*, 1988, vol. 104, pp. 1–8.
86. W. Walston, I. Bernstein, and A. Thompson: *Metall. Trans. A*, 1991, vol. 22, pp. 1443–51.
87. P. Caron and T. Khan: *Aerosp. Sci. Technol.*, 1999, vol. 3, pp. 513–23.
88. S. Hegde, R. Kearsey, and J. Beddoes: *Mater. Sci. Eng. A*, 2010, vol. 527, pp. 5528–38.
89. M. Schwind, J. Kallqvist, J. Nilsson, J. Agren, and H. Andren: *Acta Mater.*, 2000, vol. 48, pp. 2473–81.
90. J. Erneman, M. Schwind, L. Nylof, J. Nilsson, H. Andren, and J. Agren: *Metall. Mater. Trans. A*, 2005, vol. 36A, pp. 2595–2600.
91. L. Zhang and I. Steinbach: *Acta Mater.*, 2012, vol. 60, pp. 2702–10.
92. A. Malik, J. Odqvist, L. Hoglund, S. Hertzman, and J. Agren: *Metall. Mater. Trans. A*, 2017, vol. 48A, pp. 4914–28.
93. M. Avrami: *J. Chem. Phys.*, 1940, vol. 8, pp. 212–24.